# Evaluation of Critical Components of Non-Ceramic Insulators In-Service: Role of Defective Interfaces

## *Final Project Report*

**Power Systems Engineering Research Center**

*A National Science Foundation
Industry/University Cooperative Research Center
since 1996*

**Power Systems Engineering Research Center**

# Evaluation of Critical Components of Non-Ceramic Insulators (NCI) In-Service: Role of Defective Interfaces

## Final Project Report

### Project Team

Ravi Gorur, Project Leader, Arizona State University
Bob Olsen, Washington State University
Art Kroese, Salt River Project
Fred Cook, Western Area Power Administration
Senthil Kumar S., Graduate Student, Arizona State University

August 2004

**Information about this project**

For information about this project contact:

Ravi Gorur
Professor
Department of Electrical Engineering
Ira A. Fulton School of Engineering
Arizona State University
Tempe, AZ 85287-5706
Tel: 480-965-4894
Fax: 480-965-0745
Email: ravi.gorur@asu.edu


**Power Systems Engineering Research Center**

This is a project report from the Power Systems Engineering Research Center (PSERC). PSERC is a multi-university Center conducting research on challenges facing the electric power industry and educating the next generation of power engineers. More information about PSERC can be found at the Center's website: http://www.pserc.org

For additional information, contact:

Power Systems Engineering Research Center
Cornell University
428 Phillips Hall
Ithaca, New York 14853
Phone: 607-255-5601
Fax: 607-255-8871

# Acknowledgements

**Executive Summary**

This report contains the results and analysis of electric field computation performed to investigate the possibility of detecting internal defects in non-ceramic insulators (NCI) via the measurement of electric field outside the insulator. A three-dimensional commercial software package, COULOMB, has been utilized. Various type of defects have been simulated. Since most problems with NCI are related to interfaces, the defects simulated are assumed to be interfacial, i.e, residing at an interface.

The following are the conclusions:

- The defect detection is position dependent and has the best possibility of being detected if it is closer to the high voltage electrode.
- Larger and longer defects produce higher field changes. Hence, they are more easily detected than the smaller ones.
- The change in field value observed depends on the type of the defect. The more conductive the defect is, greater is the possibility of detecting it.
- The range of the field probe can be greatly enhanced if measurements are taken radially instead of conventional axial measurements.

Caution is advised on the use of electric field probes for defect detection of NCIs. There are too many limitations to use this technique (even though it is among the most powerful ones existing presently) that make it unsafe for a human operator. Further research is required to ensure that better techniques are developed in order that the process of decision making on when to replace NCIs in service is made in a safe and fool-proof manner

# Table of Contents

# List of Figures

# List of Tables

# 1. Introduction

## 1.1 Background

Outdoor high voltage ceramic and composite (non-ceramic) insulators are used for mechanical support and to electrically isolate the transmission and distribution lines from the grounded tower as shown in Fig. 1 to Fig. 3.
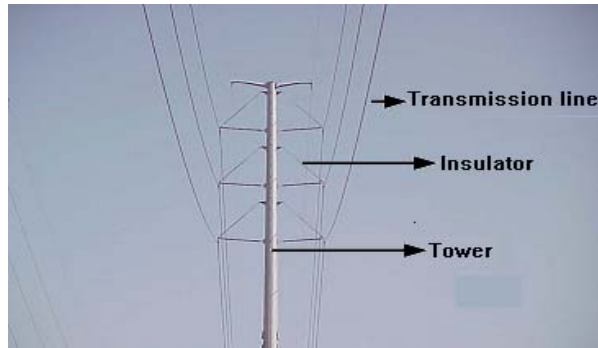


Figure 1.  Overhead Line for Power Delivery



Figure 2.  Ceramic Insulators in an Overhead Line
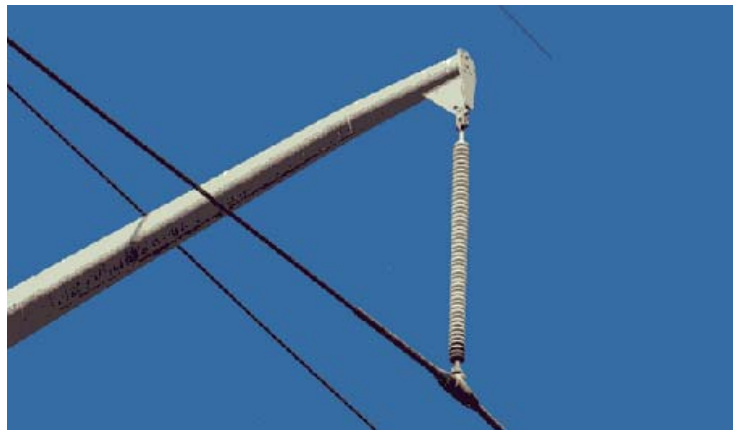


Figure 3.  Non-Ceramic Insulator in an Overhead Line

Outdoor insulators deployed are of three basic types:
   a)  Porcelain
   b)  Non-ceramic (also known as composite)
   c)  Glass.


## 1.2  Non-Ceramic Insulators

Non-ceramic insulators (NCIs) consist of a fiber glass core that provides the main mechanical strength. It is enclosed inside a protective housing with several weather sheds with two end fittings as shown in Fig. 4 [1].
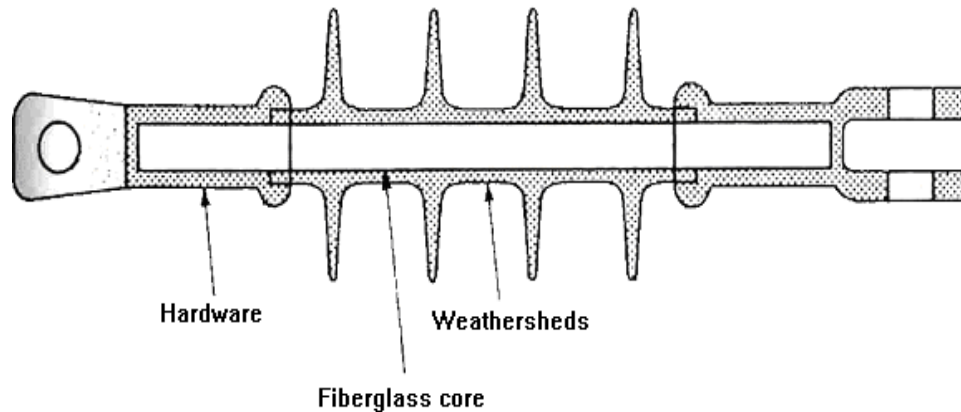


Figure 4.  Cross-section of a Non-Ceramic Insulator


The housing may be made of different materials such as EPDM, silicone rubber and epoxy depending on various constraints of contamination performance, tracking and erosion resistance, and hydrophobicity.  It can be observed from Fig. 4 that the electrodes in NCIs are isolated only by the dielectric and there are no intermediate metal parts as in ceramic insulators.  The critical interfaces in this type of insulator are (1) between the rod and housing, (2) between hardware-rod-housing, and (3) different sheds of housing if unit is not manufactured in a single piece.

Electrical discharges that produce partial breakdown of air gap is called corona.  The presence of corona at the interfaces leads to sheath damage exposing the fiberglass rod, tracking the rod, thereby leading to insulator failure through interfacial flashover.  The presence of high field stresses is the cause of corona.  Also, the presence of any contamination like water, salts, and dirt can intensify the field at those locations.

## 2. Electric Field and NCIs

Understanding the electric field distribution plays a vital role in insulator design [2]. In addition, field studies can be useful for detecting internal defects. In ceramic insulators the voltage distribution is relatively more linear due to the presence of intermediate metal parts. The material does not degrade with corona; hence, corona is not a problem in ceramic insulators. However, in NCIs, the voltage distribution is highly non-uniform as shown in Fig. 5, and can give rise to corona. Corona rings are normally used for NCI at voltages above 230 kV in order to reduce the electric field near the line end.
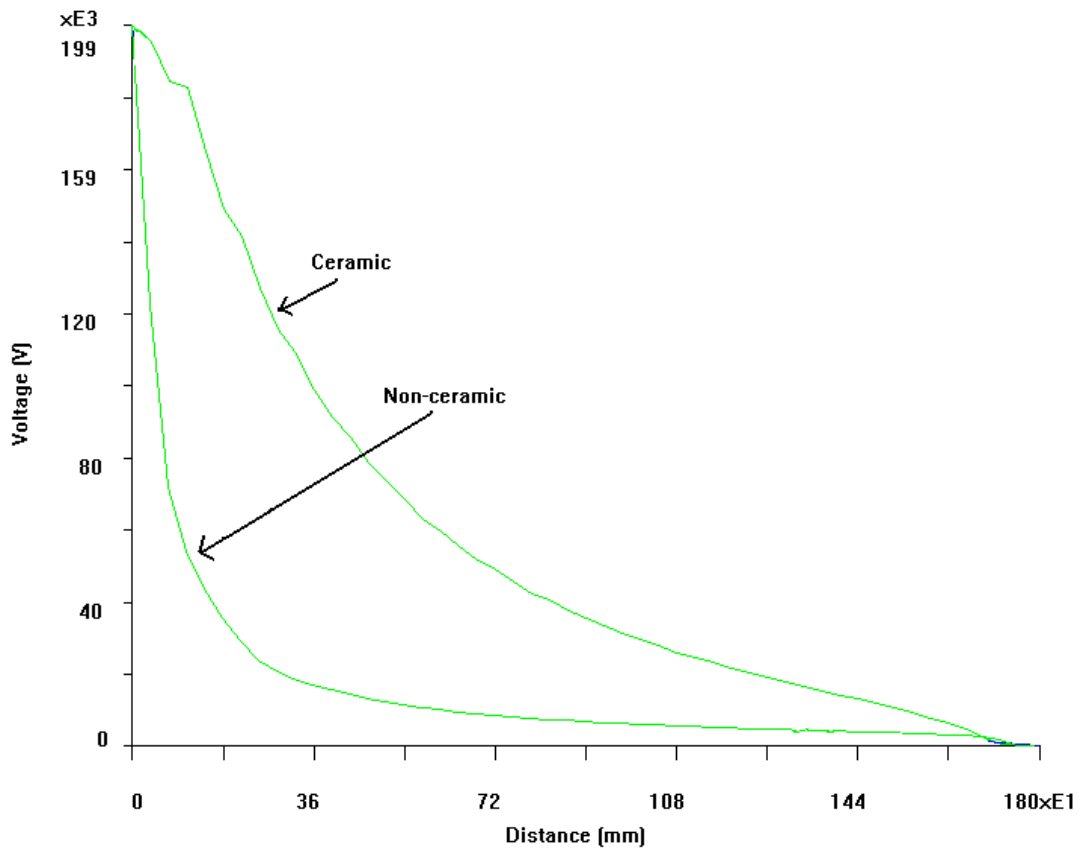


Figure 5. Comparison of Voltage Distribution in Ceramic and Non-Ceramic Insulators

The effect of corona can be seen by comparing field distributions for NCI's with and without corona rings from Fig. 6 and Fig. 7 respectively. It could be seen that for insulators with corona ring, the peak field intensity is reduced considerably and field distribution is made more uniform.

3
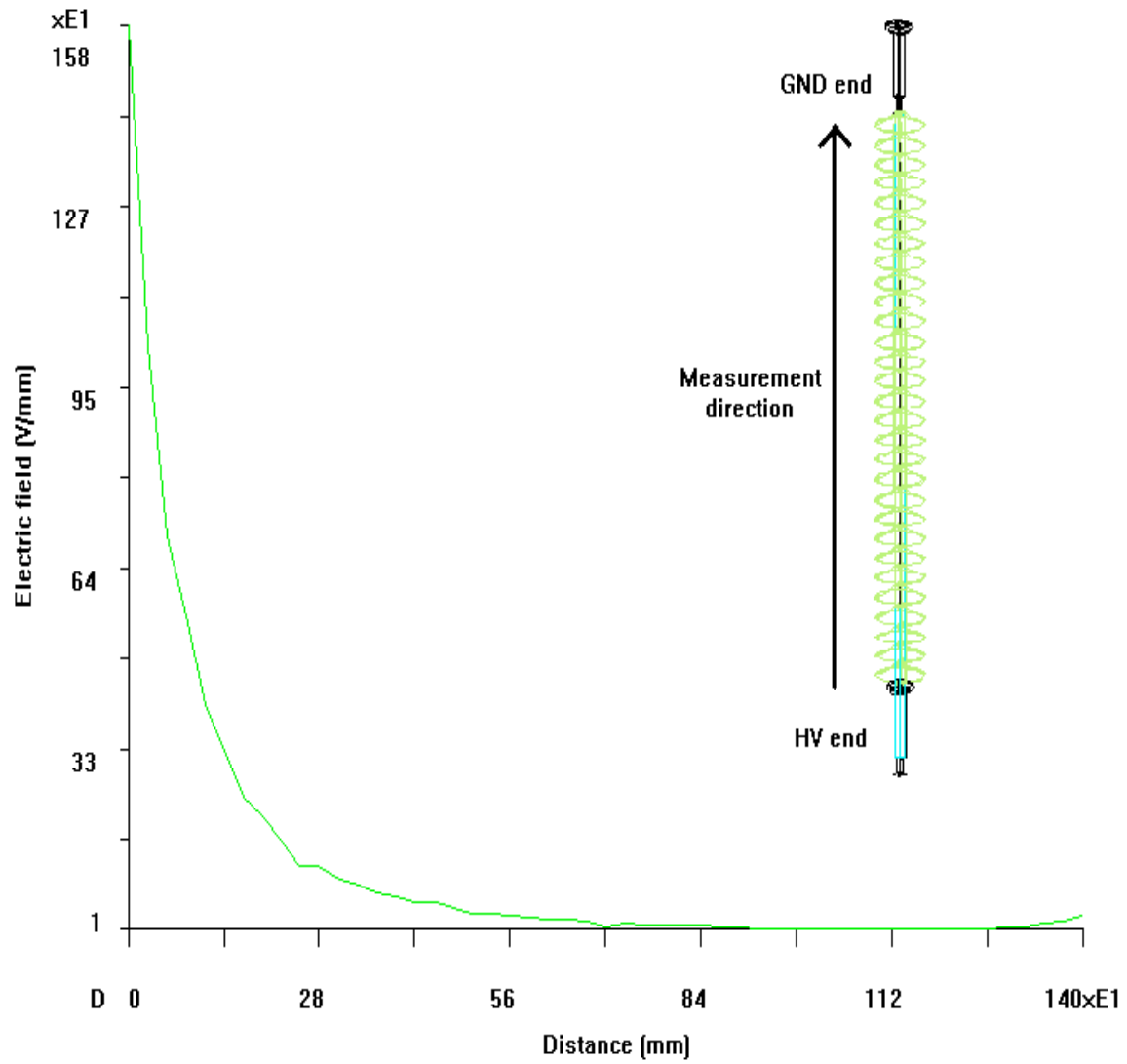
Figure 6.  Field Distributions along a Non-Ceramic Insulator without Corona Ring.
Insulator dimensions are obtained from Ref [3].

It could be observed that the field intensity near the high voltage end is considerably reduced.  Higher system voltages require larger dimensions for the corona ring.

4
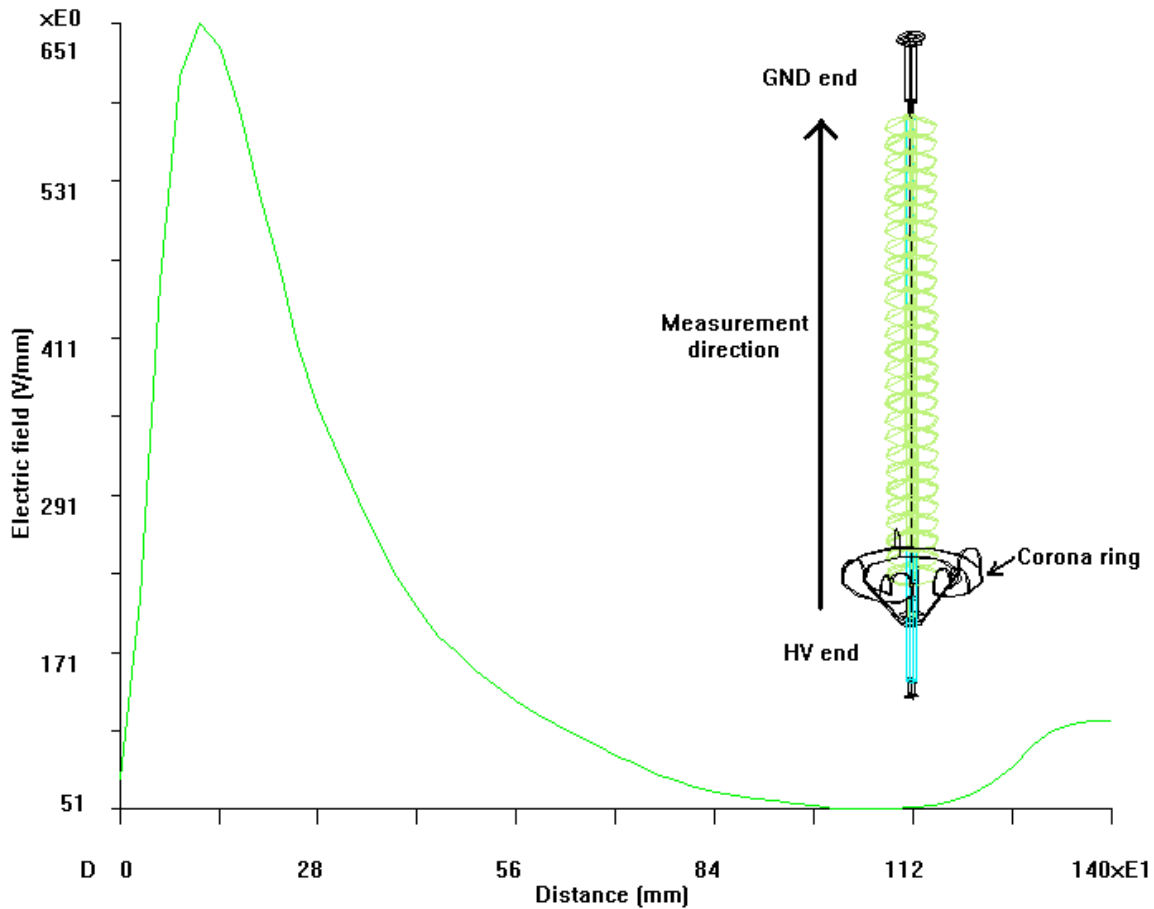
Figure 7. Field Distributions along a Non-Ceramic Insulator with Corona Ring

Effective methods are needed to identify faulty insulators and replace them on time before a failure occurs. Several methods have been proposed for the detection of insulator defects but electric field method is the most promising of all because it provides a method of detecting internal defects. Defects can cause a change in the material property that reflects as a change in the electric field. However, all defects do not cause a significant change in the electric field suitable for detecting it. Hence, there is a need to characterize the field method based on defect sizes, defect properties and locations. Understanding the limitations of this technique is necessary to know how early and how large a defect could be identified during maintenance.

Thus electric field studies are important for insulator design as well as for defect identification during periodic maintenance of transmission lines.

## 3.  Electric Field Analysis Method Used in Project

Analysis of electric fields can be done using various numerical techniques.  Each method has several advantages and limitations depending on the nature of the problem.  The method should be capable of handling three-dimensional geometries and various material types so that the environmental conditions of the apparatus could be taken into account.

These methods involve modeling the entire geometry either in a one, two or three-dimensional space using appropriate differential/integral equations and solving them [4-6].  The computations are complex and hence computers are a necessity for these methods.  The computation time increases with increased accuracy.  Hence, there is generally a tradeoff between time and accuracy.

### 3.1  Boundary Element Method (BEM)

In this method, the partial differential equations governing the solution in a domain are replaced by equations governing just the boundary [6]. Consider a boundary as shown in Fig. 8. The boundary is first approximated using panels.  The panels are straight lines in the case of two-dimensional boundaries, triangles in the case of three-dimensional boundaries and truncated cones in the case of an axis symmetric problem.  Integral equations are then formulated from the partial differential equations using either a direct or an indirect method.

In direct method, solving the Laplace's equation $\nabla^2 \phi = 0$ governing the interior to a domain D bounded by a surface S, the partial differential equation is replaced by

$$\int_S \frac{\partial G}{\partial n_q}(p,q)\phi(q)ds_q + \frac{1}{2}\phi(q)$$

(1)

$$\int_S G(p,q)\frac{\partial \phi}{\partial n_q}ds_q$$

(2)

where G is the Greens function defined by the dimension of the domain.
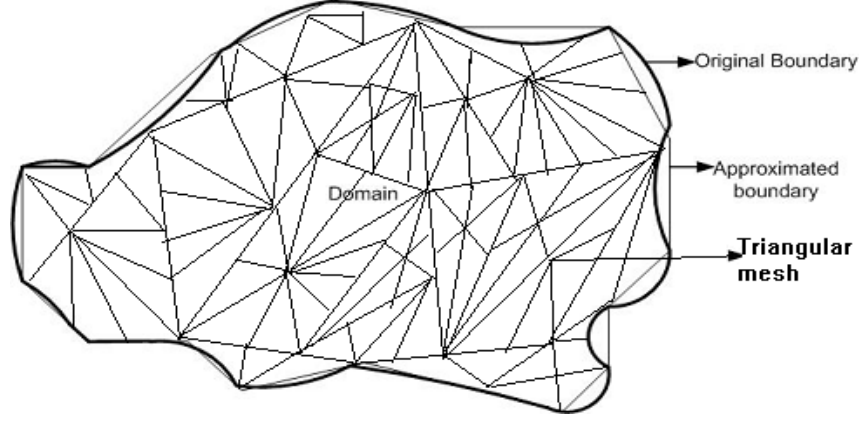
Figure 8. Boundary Approximation in BEM

For a two dimension domain,

$$G(p,q) = -\frac{1}{2\Pi}\log r$$

(3)

For a three dimension domain,

$$G(p,q) = \frac{1}{4\Pi r}$$

(4)

Here $G(p, q)$ represent the effect observed at a point $p$ due to a unit source at a point $q$. Equation (3) is now represented as an integral equation using operator notations as

$$\{M\phi\}_S(p) + \frac{1}{2}\phi(p) = \{LV\}_S(p)$$

Where $V(q) = \dfrac{\partial \phi}{\partial n_q}$

(5)

$$\{M\xi\}\Gamma(p) \equiv \int_\Gamma \frac{\partial G}{\partial n_q}(p,q)\xi(q)ds_q$$

(6)

$$\left\{\left(M + \frac{1}{2}\right)\phi\right\}_S(p) = \{LV\}_S(p)$$

(7)

where M is the integral operator, $\Gamma$ is the domain of integration, and

$$(L\xi)_S(P) = V(p) \tag{8}$$

In the indirect method of integral equation formulation, it is assumed that the solution could be expressed in terms of a source density function defined on the boundary concerned as in (9),

$$\phi(p) = \int_S G(p,q)\sigma(q)ds_q \tag{9}$$

where $\sigma$ is the source density function defined on the boundary S. The integral equation is then obtained as

$$\frac{\partial \phi}{\partial n_p}(p) = \int_S \frac{\partial G}{\partial n_p}(p,q)\sigma(q)dS_q + \frac{1}{2}\sigma(p) \tag{10}$$

The operator notation for the (10) is

$$\phi(p) = \{L\sigma\}(p) \tag{11}$$

$$v(p) = \left\{\left(M^t + \frac{1}{2}I\right)\sigma\right\}(p) \tag{12}$$

where $M^t$ is the transpose of $M$.

The integral equations are then converted into a linear system of equations using a quadrature formula or a weighted residual method such that

$$M\hat{\phi} + \frac{1}{2}\hat{\phi} = L\bar{V} \tag{13}$$

The vector components of $\underline{\phi}$ and $\underline{V}$ represents the values of the function $\phi(p)$ and $\partial\phi/\partial n_q(p)$. The solution of the integral equation provides the unknown boundary functions on S. Hence

$$\phi(p) = \int_S G(p,q)\frac{\partial \phi}{\partial n_q}ds_q - \int_S \frac{\partial G}{\partial n_q}(p,q)\phi(q)ds_q \tag{14}$$

$$\phi(p) = \{L\phi\}_S - \{Mv\}_S \tag{15}$$

This method can be used for complicated shapes and problems of large size without a significant increase in the number of elements. Hence, problems that consume a lot of time when solved using other methods could be done much faster using BEM. However, since the boundary is approximated using panels, it adds inaccuracies. The input panels needs to be checked to ensure that their sizes are reasonably uniform and the input boundary must be verified so that they do not contain sharp angles that might increase the potential that point. Increased number of elements needs to be added to areas with intricate shapes in order to avoid inaccuracies.

## 3.2  Advantages of Three-Dimensional Over Two-Dimensional Modeling

Modeling and analysis of simple, symmetrical geometries in 2-D coordinates gives fairly accurate results. However, for intricate shapes such as an outdoor insulator, modeling in 3-D provides better verification of the dimensions of the actual model. From the analysis perspective, 3-D modeling ensures that the entire information about a model is investigated thoroughly unlike in 2-D models where information about one coordinate is not taken into account.

3-D modeling also ensures that only one model is required unlike in 2-D where models for different views (top view, front view and side views) are needed to describe the complete model. Therefore, multiple analyses are a necessity for 2-D methods that increase the design time.

Hidden and overlapping surfaces result in erroneous solutions. In 2-D modeling, the presence of such surfaces cannot be identified. However, in 3-D modeling such surfaces can be easily identified and appropriate modifications can be done before analysis.

# 4.  Comparison of Methods Used for Identification of Insulator Defects

Several methods have been identified for the detection of defects in live line and in laboratory conditions [7]. Methods common in practice are buzz method, resistance method using a megger, guarded and unguarded dielectric current measurements, partial discharge measurements, RIV measurements, time withstand tests, heating tests, infrared thermography and electric field method.

## 4.1  The Buzz Method (for porcelain insulators)

In this method the voltage across a bell is applied between two sharp points on the prongs of a hot stick as in Fig. 9 [1].  The healthy insulator will provide an arc across the prongs producing a buzz sound.  A defective shed on the other hand will not have enough potential to produce such an arc.
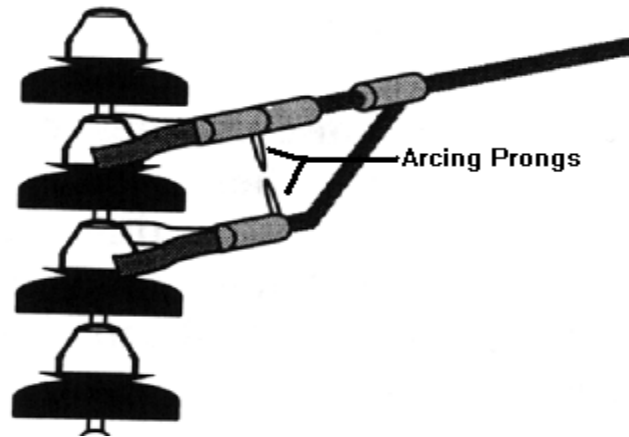


Figure 9.  Buzz Method of Testing Ceramic Insulators

This method can be used only for ceramic insulators because of the presence of metal parts upon which the electrodes can be placed.

## 4.2  Megger-Based Resistance Method

The resistance between any two points of the insulator can be measured using a high voltage megger.  Different sections and lengths of the insulator are measured for resistances.  The presence of a low resistance will indicate the presence of a defect.  This method can be used for both ceramic and non-ceramic insulators in the laboratory and not suitable for field use.  This method is useful only for surface defects and very large conductive internal defects.  Tracks of smaller lengths cannot be detected using this method.

## 4.3 Dielectric Current Measurements

The AC dielectric current that flows through an energized insulator will be through its surface as well as through its body. This current will have both the capacitive and resistive components. In addition there is a stray air capacitance current that flows between the end fittings. In order to measure the current flowing through the insulator, the stray air capacitance is eliminated using a guard electrode and the dielectric current is obtained using the shunt resistance method. The presence of high currents indicates the presence of defects. This method can be used in the lab can be adapted to the field for both ceramic and non-ceramic insulators. However, this method was found to detect only large defects that could cause an immediate failure and not smaller potential defects. Hence, this method cannot be used as a reliable test technique.

## 4.4 Partial Discharge Method

The presence of concentrated field locations can cause discharges and corona. These discharges can be detected using partial discharge measurements in which the insulators are grounded through the partial discharge apparatus. A filter identifies the discharges occurring on the insulator in the form of current pulses. The current pulses are integrated over time to obtain the charge of the partial discharge. The discharges in a healthy insulator are very less and in the order of few pico coulombs. Heavier discharges would indicate the presence of field concentrations and corona. This method is though effective is highly prone to noise and hence can be used only in a Faraday's cage and not in an outdoor environment.

## 4.5 RIV Measurements

In this method, a parabolic dish with a very sensitive microphone and a high gain amplifier are used to hear the noise produced due to corona. Background noise has found to interfere with this apparatus. The presence of corona can be a source of defect. However, this method is not a very reliable technique for defect identification, as the location of corona cannot be spotted.

## 4.6 Time Withstand/Heating Tests

This is a lab test that could be performed on both ceramic and non-ceramic insulators. The insulators are subjected to 80% of their measured flashover voltage for several minutes. The insulators are then de-energized and examined for general and localized heating. The presence of hot spots would indicate the presence of defects.

## 4.7 Dry Lightning Impulse Withstand Tests

The impulse method works on the principle of applying a standard impulse voltage with a suitable magnitude and a rise/fall time period of 1.25/50 μs to the insulator and monitoring the voltage across the insulator. A healthy insulator will have a linear voltage rise for 1.25 μs followed by an exponentially decaying voltage for 50 μs. The presence

of a short circuit will result in a voltage collapse. This method can be used for both ceramic and non-ceramic cases but only in a laboratory.

## 4.8 Infrared Thermography

Ceramic and non-ceramic insulators can be observed for defects using this method. A healthy ceramic insulator produces heating near the pin area during wet conditions such as during washing unlike a punctured unit that will remain cold. By using thermo vision equipment the presence of hot and cold areas could be identified that could be used for defect detection. In non-ceramic insulators, the temperature distribution from the line end to the ground end should be within $3^{o}$ C with higher temperatures closer to the ends. Any variations in the temperature range observed or the location of hotter regions away from the ends indicates the presence of defects [8].

## 4.9 Electric Field Method

The electric field along the surface of the insulator is measured by sliding a probe attached at the end of a hot stick along the insulator surface and the field values are stored in a data logger attached to the probe [9-11]. The readings are then loaded onto another computer where the measured field values are compared with a healthy case. Any significant change in the field values would indicate the presence of defects. This is one of the most commonly followed methods of fault detection by the utilities for both ceramic and non-ceramic cases.

Upon detailed investigation, it has been found that there is no single method that can effectively detect all the defects. However, the electric field method is a most promising method.

# 5.   Comparison of Methods Used for Identification of Insulator Defects

Several types of defects that can occur on a NCI were modeled.  The various types of defects that are considered difficult to detect but critical are incorporated on to the healthy model and simulated.  The size, position and conductivity of such defects are varied.  The field values for locations close to the defect along the path of the probe are noted down.  These values are then compared with the values obtained in the healthy cases.  The most sensitive electric field probes are sensitive for field values above 2 kV/m [11].  Hence defects that produce a difference of 2 kV/m and above are considered detectable while others were considered undetectable.  The differences in field values thus obtained are plotted as a function of the shed number.  A logarithmic trend line is fitted to the above plot for a better perception of the defect detection possibilities.

Various types of defects such as those occurring on the shed, shank, interface, external tracks from end fittings and tracks occurring on the rod sheath interface were considered. Most of the external defects could be observed during careful visual inspection. However, defects that occur inside the housing are not visible.  Hence, such defects are modeled for electric field distortion studies to verify the possibility of detecting such defects using field probes, as shown in Table 1.  A defect that occurs for the distance between any two consecutive sheds is named as the single-shed defect.  A single-shed defect will have the shape of a cylinder with a 9.2 cm height and 5 mm diameter.  A diagrammatic representation of various types of single shed defects modeled is as shown in Fig. 10.  Similarly two-shed and three shed defects are simulated and analyzed.

Table 1.  Various Defects Modeled in Non-Ceramic Insulators

| Defect Type | Non-Ceramic |
|---|---|
| Single-shed defect | Fully conductive defect at rod sheath interface |
|  | 100 mS/m conductive water defect at rod sheath interface |
|  | Air void defect at rod sheath interface |
| Two-shed defect | Fully conductive defect at rod sheath interface |
|  | 100 mS/m conductive water defect at rod sheath interface |
|  | Air void defect at rod sheath interface |
| Three-shed defect | Fully conductive defect at rod sheath interface |
|  | 100 mS/m conductive water defect at rod sheath interface |
|  | Air void defect at rod sheath interface |
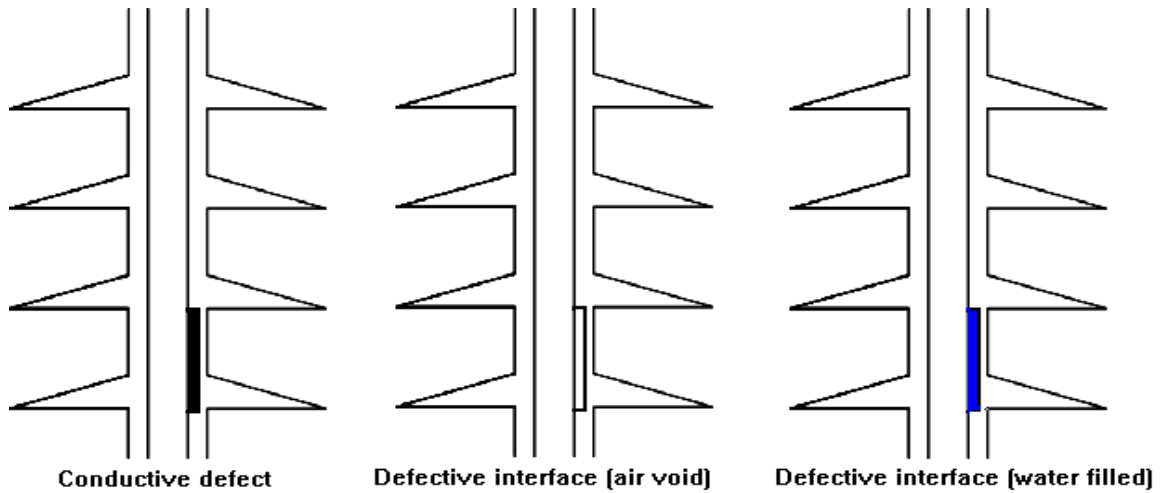
Figure 10.  Diagrammatic Representations of Various Types of Single-Shed Defects

**Axial Field Measurement along Path AB**

In this method, the field measurements on the insulator are done along the axis and surface of the sheds as indicated by the path AB in Fig. 11.  A distance of 2mm is assumed for the air gap in order to slide the probe on the insulator.  The values obtained are compared with that of a healthy insulator and the change in field value (Table 2) is plotted against the shed number.
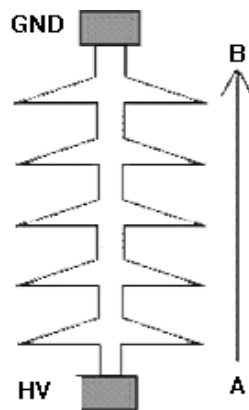


Figure 11.  Measurement along Insulator Surface from Location A to B

The single-shed defect is moved starting from the high voltage end to the ground end with an ascending order of the shed number and the change in values obtained is plotted against the shed number.  A logarithmic trend line is drawn for the different cases modeled as shown in Fig. 12.

Table 2. Change in Electric Field for Single-Shed Defects Measured Axially

| Shed number | Change in field values for a fully conductive defect | Change in field values for a air void defect | Change in field values for a water defect |
|---|---|---|---|
| | kV/m | kV/m | kV/m |
| 1 | 791.27 | 33.47 | 119.27 |
| 2 | 2.77 | 15.68 | 34.7 |
| 3 | 13.607 | 19.53 | 25.438 |
| 4 | 3.935 | 3.864 | 10.556 |
| 5 | 2.45 | 2.418 | 4.621 |
| 6 | 2.156 | 2.411 | 3.058 |
| 7 | 2.111 | 2.028 | 3.024 |
| 8 | 1.364 | 1.549 | 2.002 |
| 9 | 1.004 | 1.117 | 1.717 |
| 10 | 0.6337 | 0.7939 | 1.1937 |
| 11 | 0.8266 | 0.6484 | 1.0937 |
| 12 | 0.7033 | 0.6423 | 0.9499 |
| 13 | 0.7863 | 0.643 | 0.9003 |
| 14 | 0.5418 | 0.5209 | 0.7028 |
| 15 | 0.6042 | 0.4175 | 0.6357 |
| 16 | 0.5305 | 0.4067 | 0.6073 |
| 17 | 0.7109 | 0.427 | 0.6683 |
| 18 | 0.9262 | 0.6889 | 0.862 |
| 19 | 1.4508 | 1.1155 | 1.2932 |
| 20 | 13.07 | 1.4267 | 1.399 |
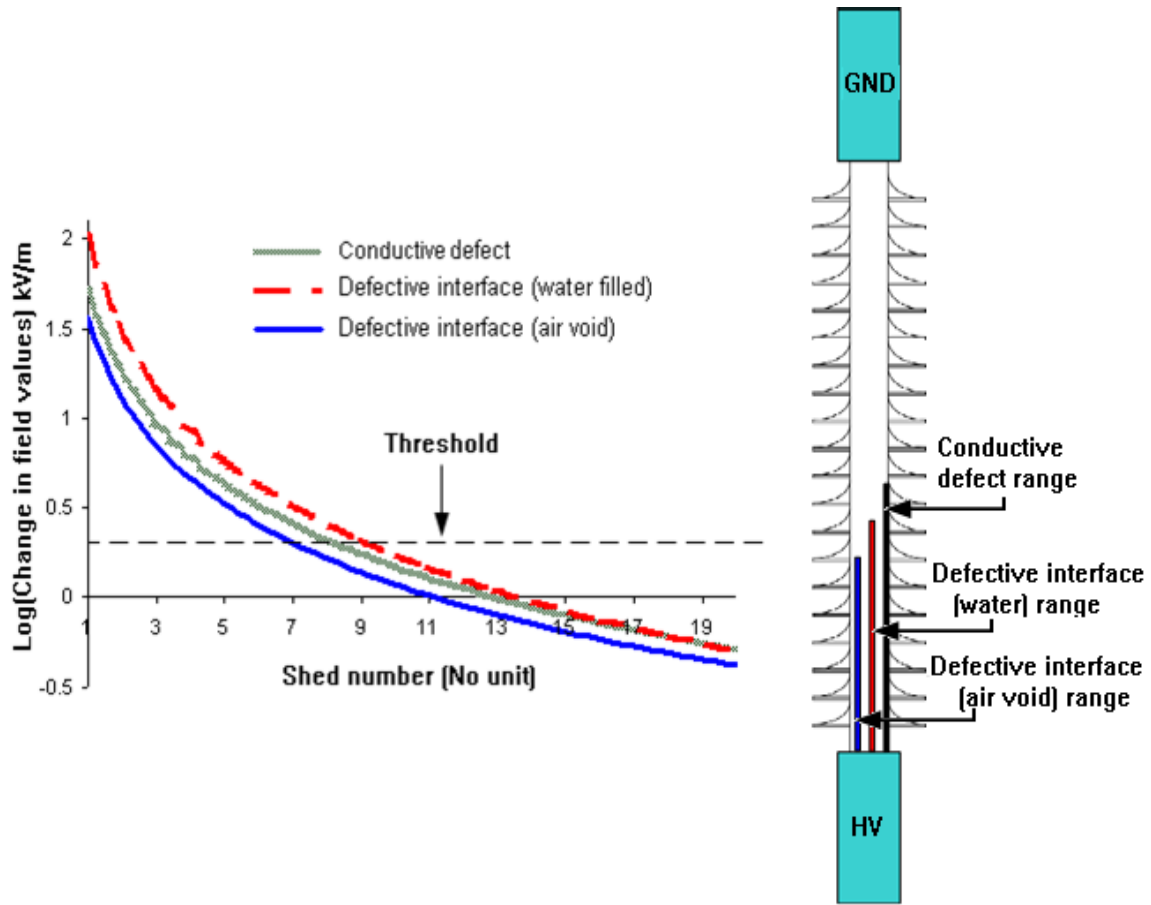
Figure 12.  Trend Lines for Axial Single-Shed Defect Measurements

A two-shed defect with an 18.4cm height with a 5mm diameter is placed on a healthy 345 kV line insulator.  The defect is positioned for different shed numbers as well as for different material compositions as in the single shed case.  The change in field values observed is tabulated (Table 3) and a trend line is plotted as shown in Fig. 13.

Table 3.  Change in Electric Field for Two-Shed Defects Measured Axially

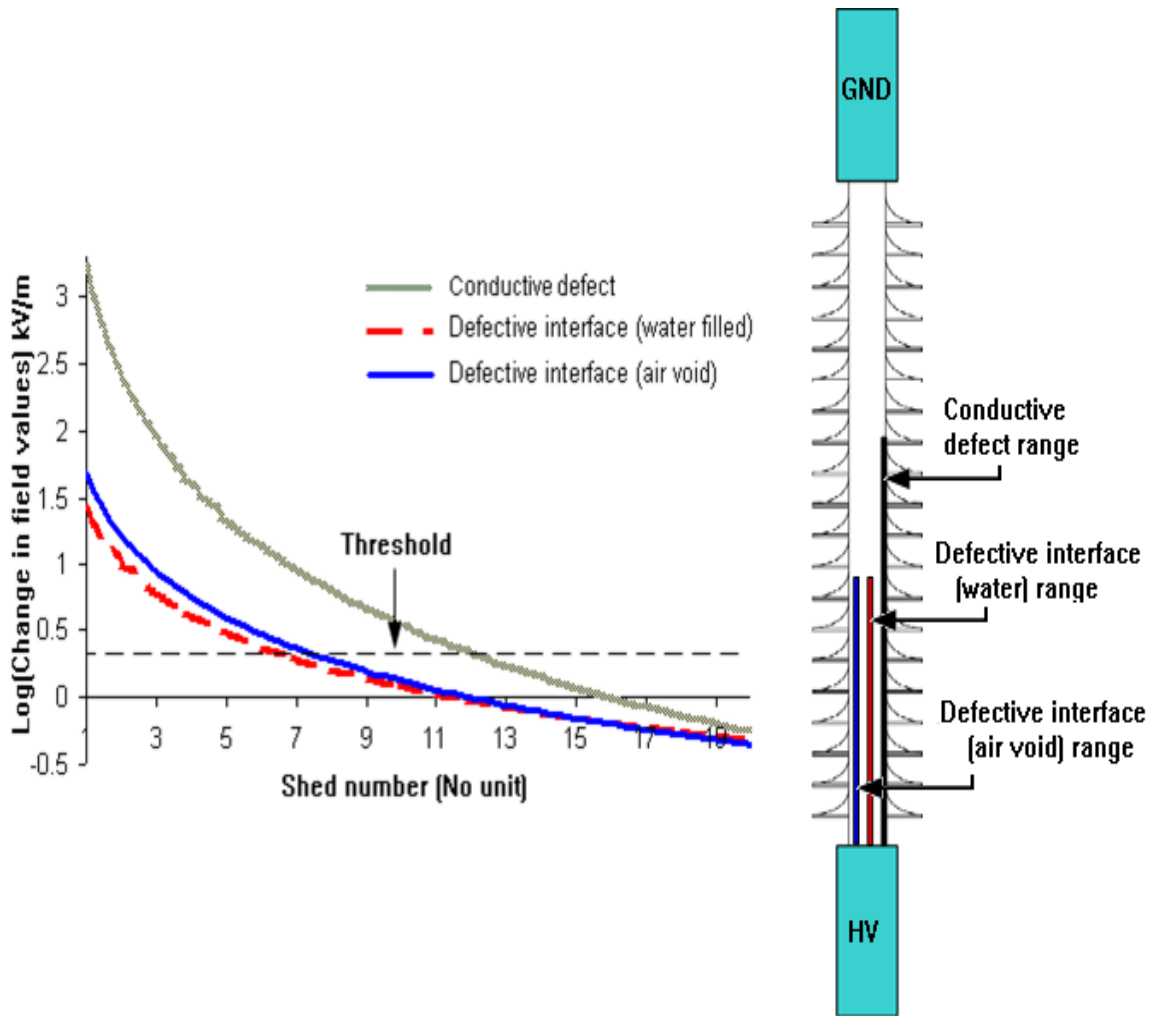| Shed number | Change in field values for a fully conductive defect | Change in field values for a air void defect | Change in field values for a water defect |
|---|---|---|---|
| | kV/m | kV/m | kV/m |
| 1 | 801.97 | 35.89 | 22.55 |
| 2 | 1023.48 | 39.18 | 6.46 |
| 3 | 90.27 | 20.246 | 13.451 |
| 4 | 32.402 | 4.149 | 73.128 |
| 5 | 29.689 | 2.556 | 6.193 |
| 6 | 16.611 | 2.758 | 2.827 |
| 7 | 8.201 | 2.182 | 0.67 |
| 8 | 4.866 | 1.71 | 0.437 |
| 9 | 3.994 | 1.23 | 0.357 |
| 10 | 3.68 | 0.9017 | 1.7817 |
| 11 | 2.5104 | 0.7363 | 0.0396 |
| 12 | 2.175 | 0.7214 | 1.6875 |
| 13 | 1.2074 | 0.7033 | 0.5879 |
| 14 | 1.2983 | 0.5788 | 1.0329 |
| 15 | 0.8586 | 0.4687 | 0.0553 |
| 16 | 0.9579 | 0.4539 | 0.5422 |
| 17 | 0.4246 | 0.4776 | 0.7215 |
| 18 | 0.1193 | 0.7421 | 0.7897 |
| 19 | 0.7512 | 1.1847 | 1.2711 |
| 20 | 13.73 | 1.5616 | 21.303 |

Figure 13.  Trend Lines for Axial Two-Shed Defect Measurements

In a three-shed case the cylindrical defect has a 28.2 cm height with a 5 mm diameter.  The defect is placed at different shed locations as well as for different material compositions as in the previous cases.  The results are tabulated (Table 4) and a trend line is plotted as shown in Fig. 14.

Table 4.  Change in Electric Field for Three-Shed Defects Measured Axially

| Shed number | Change in field values for a fully conductive defect | Change in field values for a air void defect | Change in field values for a water defect |
|---|---|---|---|
| | kV/m | kV/m | kV/m |
| 1 | 718.67 | 36.2 | 24.04 |
| 2 | 1078.28 | 39.33 | 371.15 |
| 3 | 1122.5 | 20.716 | 170.62 |
| 4 | 143.318 | 4.173 | 3.593 |
| 5 | 62.521 | 2.468 | 1.043 |
| 6 | 47.239 | 2.768 | 5.014 |
| 7 | 7.303 | 2.287 | 3.05 |
| 8 | 17.917 | 1.693 | 1.789 |
| 9 | 12.467 | 1.23 | 0.608 |
| 10 | 10.483 | 0.8939 | 0.9793 |
| 11 | 8.1754 | 0.7315 | 0.3258 |
| 12 | 6.8434 | 0.726 | 0.8379 |
| 13 | 4.9034 | 0.708 | 0.4236 |
| 14 | 3.9662 | 0.599 | 0.599 |
| 15 | 3.2594 | 0.4724 | 0.5052 |
| 16 | 3.1742 | 0.456 | 0.5843 |
| 17 | 2.4595 | 0.4804 | 0.7093 |
| 18 | 1.864 | 0.742 | 0.8396 |
| 19 | 0.7919 | 1.1845 | 1.3688 |
| 20 | 12.001 | 1.564 | 1.71 |
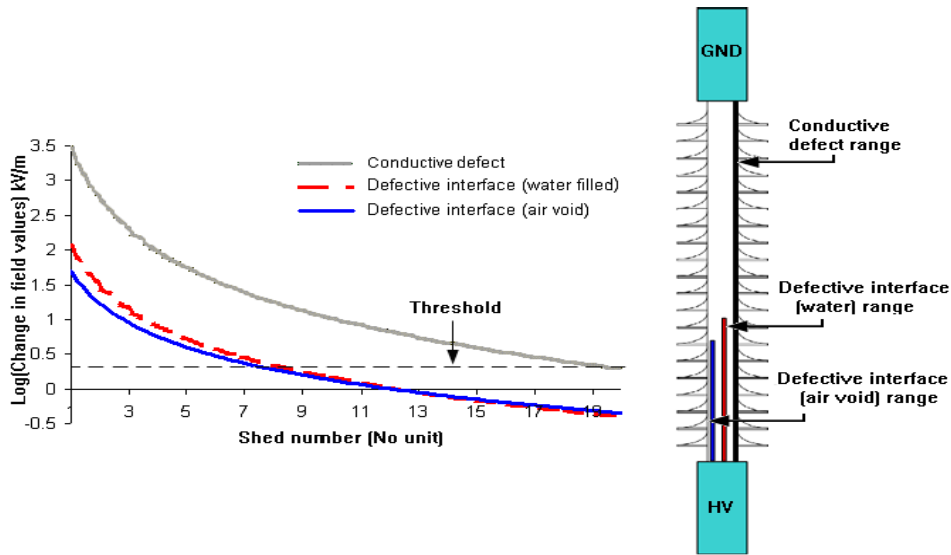


Figure 14.  Trend Lines for Axial Three-Shed Defect Measurements

**Radial Field Measurement Along Path CD**

It was observed from the simulation results that closer the probe to the defect location, greater is the field change observed. Measurements were carried out radially through the path CD as shown in Fig. 15 for the different defects and locations. A distance of 2 mm is allotted for the air gap in order to measure the field values using a probe in the radial direction.



Figure 15. Radial Field Measurements along path CD

For the single shed defects, measurements are done along the radial path CD. The changes are computed and tabulated (Table 5). The trend lines are plotted as shown in Fig. 16.

Table 5.  Change in Electric Field for Single-Shed Defects Measured Radially

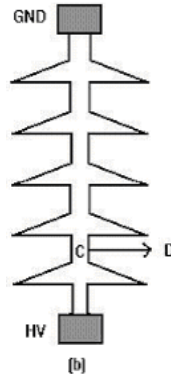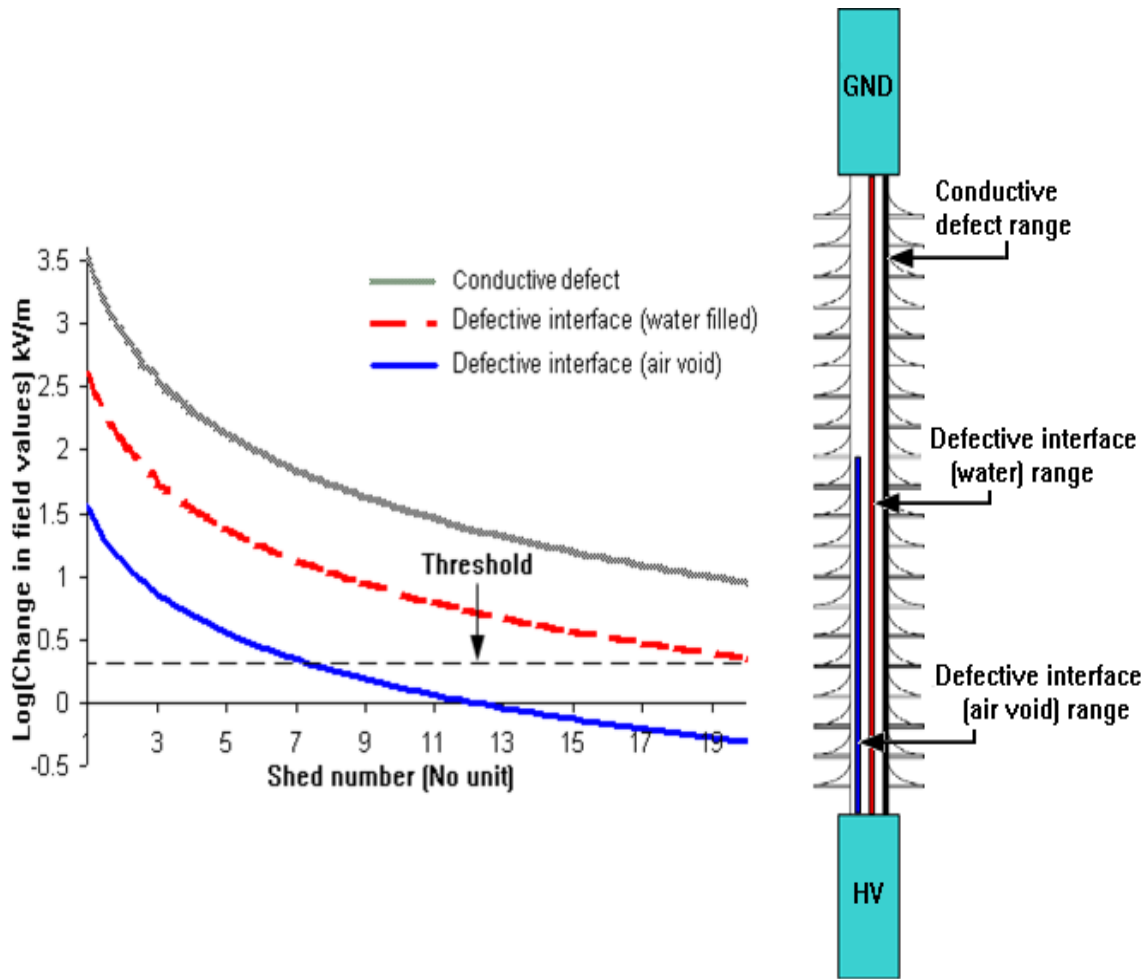| Shed number | Change in field values for a fully conductive defect | Change in field values for a air void defect | Change in field values for a water defect |
|---|---|---|---|
| | V/mm | V/mm | V/mm |
| 1 | 7624.21 | 14.01 | 2018.21 |
| 2 | 511.01 | 28.7 | 69.92 |
| 3 | 289.9 | 38.35 | 33.64 |
| 4 | 294.084 | 8.794 | 27.983 |
| 5 | 174.472 | 0.999 | 13.125 |
| 6 | 87.249 | 4.066 | 29.046 |
| 7 | 49.896 | 3.157 | 4.829 |
| 8 | 50.812 | 1.729 | 17.222 |
| 9 | 33.431 | 1.178 | 6.548 |
| 10 | 30.602 | 0.512 | 7.645 |
| 11 | 18.934 | 0.467 | 0.819 |
| 12 | 17.974 | 0.8248 | 4.624 |
| 13 | 13.6337 | 1.1419 | 4.2957 |
| 14 | 13.8459 | 0.6109 | 6.5439 |
| 15 | 11.9274 | 0.5325 | 4.4514 |
| 16 | 11.6174 | 0.4017 | 2.5139 |
| 17 | 9.9637 | 0.0301 | 3.1606 |
| 18 | 9.2639 | 1.6251 | 2.5317 |
| 19 | 10.552 | 3.7401 | 3.52 |
| 20 | 125.954 | 3.143 | 23.854 |

Figure 16.  Trend Lines for Radial Single-Shed Defect Measurements

Radial measurements are done on two-shed defective insulators and the changes in field observed are tabulated (Table 6).  The trend lines are then plotted as shown in Fig. 17.

Table 6.  Change in Electric Field for Two-Shed Defects Measured Radially

| Shed number | Change in field values for a fully conductive defect | Change in field values for a air void defect | Change in field values for a water defect |
|---|---|---|---|
| | V/mm | V/mm | V/mm |
| 1 | 5781.51 | 14.17 | 66.23 |
| 2 | 8754.11 | 132.17 | 106.76 |
| 3 | 1122.61 | 39.33 | 27.73 |
| 4 | 563.104 | 8.323 | 32.212 |
| 5 | 391.262 | 1.726 | 20.066 |
| 6 | 279.009 | 3.482 | 8.735 |
| 7 | 126.532 | 3.489 | 1.781 |
| 8 | 116.494 | 2.44 | 8.604 |
| 9 | 69.528 | 1.286 | 1.293 |
| 10 | 68.274 | 0.709 | 6.434 |
| 11 | 44.177 | 0.541 | 3.008 |
| 12 | 43.849 | 0.9213 | 1.9386 |
| 13 | 31.1937 | 1.214 | 3.1593 |
| 14 | 26.2159 | 0.6804 | 7.5439 |
| 15 | 27.2714 | 0.5827 | 2.2026 |
| 16 | 25.8224 | 0.4479 | 3.5725 |
| 17 | 26.1017 | 0.0246 | 1.1873 |
| 18 | 24.2299 | 1.7105 | 1.4082 |
| 19 | 26.556 | 3.919 | 3.06 |
| 20 | 108.584 | 3.543 | 1.858 |

23

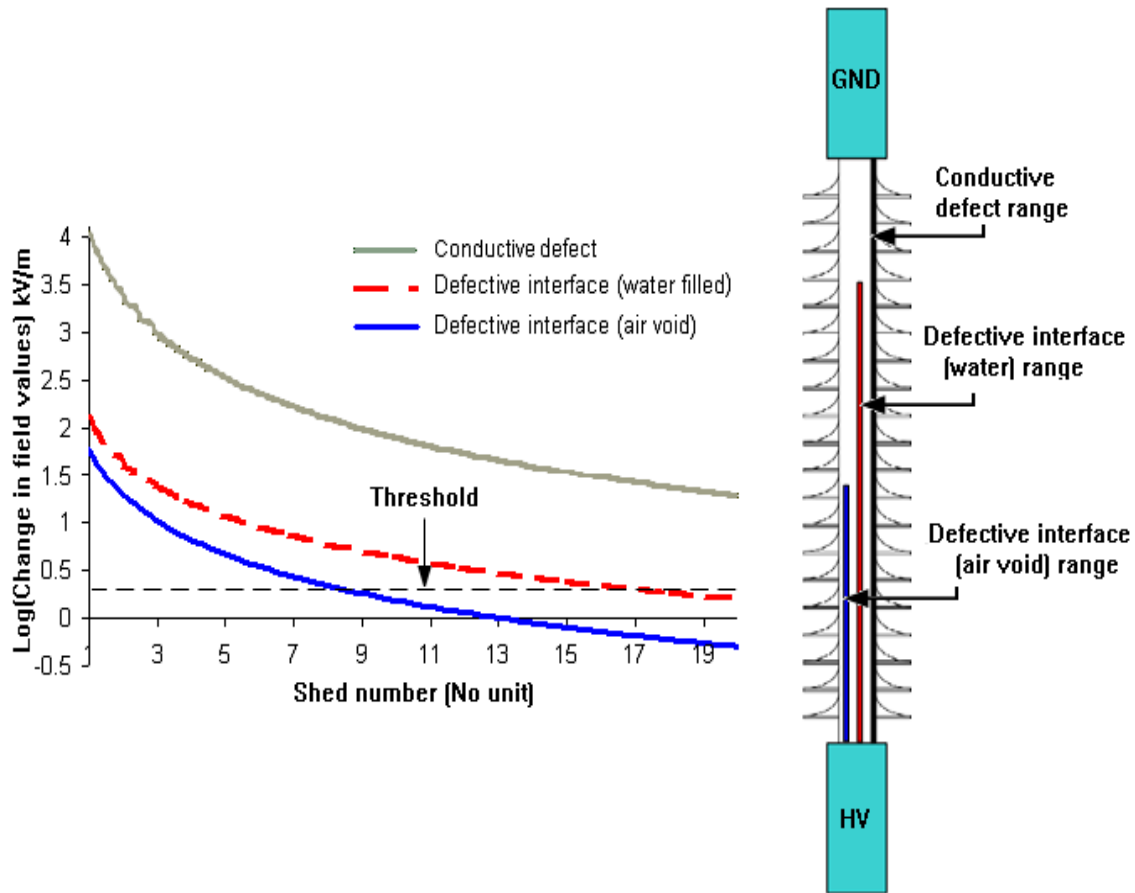Figure 17.  Trend Lines for Radial Two-Shed Defect Measurements

The results for the three- shed cases are tabulated (Table 7).  Trend lines similar to the previous two cases are plotted for the three-shed defect as in Fig. 18.  The results show that significant differences could be seen for various types of defects if measurements are done along the radial direction instead of the axial direction [12,13].

Table 7.  Change in Electric Field for Three-Shed Defects Measured Radially

| Shed number | Change in field values for a fully conductive defect | Change in field values for a air void defect | Change in field values for a water defect |
|---|---|---|---|
| | V/mm | V/mm | V/mm |
| 1 | 4997.21 | 13.36 | 4480.81 |
| 2 | 7159.41 | 131.9 | 2385.81 |
| 3 | 934.11 | 39.98 | 1691.91 |
| 4 | 415.444 | 7.657 | 148.854 |
| 5 | 311.932 | 1.648 | 71.292 |
| 6 | 204.699 | 3.553 | 15.051 |
| 7 | 84.252 | 3.781 | 13.731 |
| 8 | 66.908 | 2.417 | 0.8 |
| 9 | 35.236 | 1.302 | 0.475 |
| 10 | 36.213 | 0.698 | 3.032 |
| 11 | 20.352 | 0.51 | 3.069 |
| 12 | 17.23 | 0.9516 | 0.3358 |
| 13 | 19.2747 | 1.2348 | 1.5787 |
| 14 | 10.9419 | 0.9048 | 0.9048 |
| 15 | 17.3624 | 0.5964 | 3.0688 |
| 16 | 10.9134 | 0.4495 | 1.3463 |
| 17 | 17.7737 | 0.015 | 4.8467 |
| 18 | 13.5539 | 1.7305 | 1.3548 |
| 19 | 114.854 | 2.851 | 27.591 |
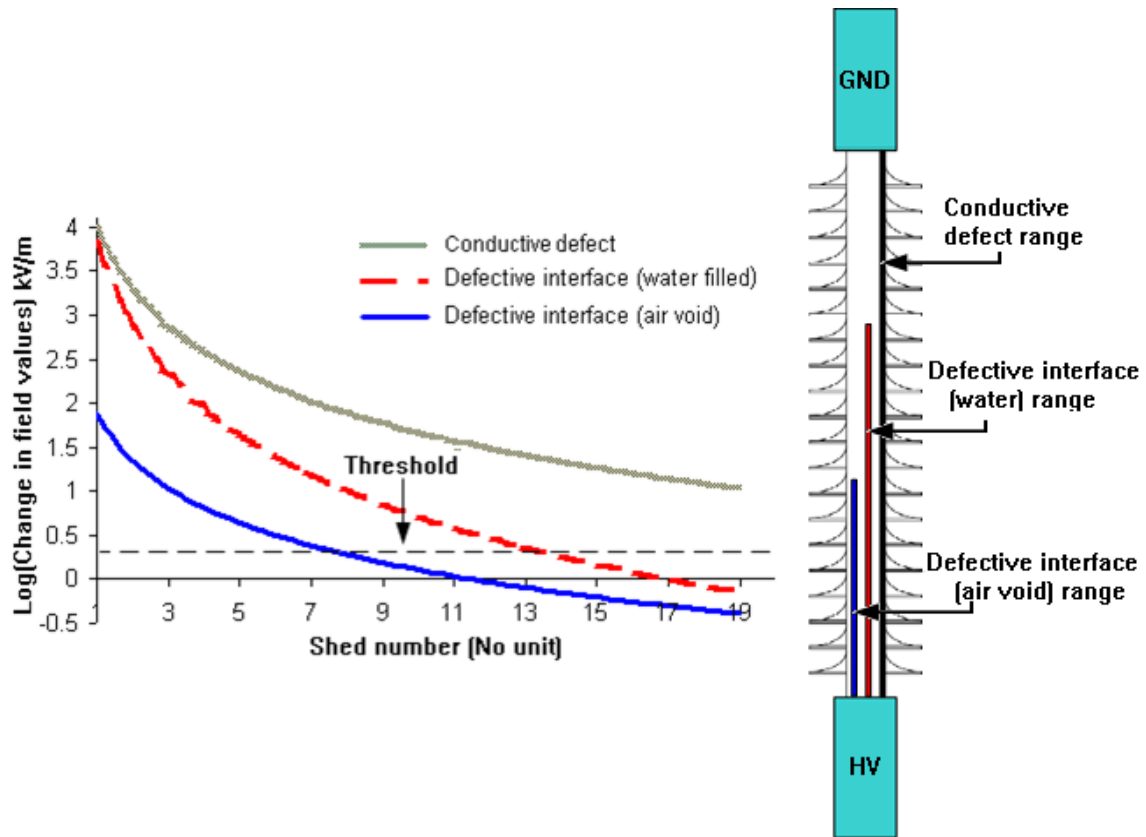
Figure 18.  Trend Lines for Radial Three-Shed Defect Measurements

The possibility of detecting defects increases if radial measurements are done instead of the axial method.  From the above results the defect detection possibilities for both axial and radial field measurement methods for a non-ceramic insulator is summarized and shown in Table 8.

Table 8.  Summary of Defect Detection Possibilities in NCIs

| Defect type | Defect Property | Axial method | | Radial method | |
|---|---|---|---|---|---|
| | | Detectable | Non-detectable | Detectable | Non-detectable |
| NCI single-shed | Fully conductive | 1 – 7, 20 | 8 – 19 | 1 – 20 | N. A |
| | Conductive water | 1–8 | 9–20 | 1–10, 12–20 | 11 |
| | Air void | 1–8 | 9 – 20 | 1–7, 19–20 | 8–18 |
| NCI two-shed | Fully conductive | 1–12, 20 | 13–19 | 1–20 | N. A |
| | Conductive water | 1–6, 20 | 7–19 | 1–6, 8,10,11,13,14,15, 16,19,20 | 7, 9,12,17,18 |
| | Air void | 1–7 | 8–20 | 1–8, 19,20 | 9–18 |
| NCI three-shed | Fully conductive | 1–17, 20 | 18,19 | 1 – 20 | N. A |
| | Conductive water | 1–7 | 8–20 | 1-7, 10,11,15,17 | 8,9,12–14, 16,18 |
| | Air void | 1–7 | 8–20 | 1–8,19,20 | 9–18 |

# 6. Conclusions and Future Work

## 6.1 Conclusions

- The defect detection is position dependant and has the best possibility of being detected if it is closer to the high voltage electrode.
- Larger and longer defects produce higher field changes hence they are more easily detected than the smaller ones.
- The change in field value observed depends on the type of the defect. More conductive the defect is, greater is the possibility of detecting it.
- The range of the field probe can be greatly enhanced if measurements are taken radially instead of conventional axial measurements.

## 6.2 Future Work

- Embedded field sensors using micro electro-mechanical systems may be able to sense minute defects such as water ingress into the fiberglass core that can provide can early warning for maintenance.
- Scanning techniques need to be explored as they can expose the anatomy of the insulator. The location and size of the defect can then be pinpointed.

# 7. References

[1] R. S. Gorur, E. A. Cherney, and J. T. Burnham, *Outdoor insulators*, Arizona, USA:Ravi S. Gorur, Inc., ISBN 0-9677611-0-7, 1999.

[2] J. J. LaForest, *EPRI transmission line reference book*, EPRI, Publication number EL-2500, 1987.

[3] *Rodurflex polymer insulator catalog*, LAPP industries.

[4] E. Kuffel, and W. S. Zaengl, *High voltage engineering*, Pergamon press, ISBN 0-08-024213-X, 1988.

[5] Matthew N. O. Sadiku, *Elements of electromagnetics*, Oxford university press, ISBN 0-19-513477-X, 2003.

[6] Stephen Kirkup. (2003 Nov.). *The BEM for Laplace problems* [Online]. Available: http://www.boundary-element-method.com/bemlap/manual.htm.

[7] IEEE task force on electrical testing of polymer insulators for hot line installation, "Electrical test methods for non-ceramic insulators used for live line replacement," *IEEE Trans. Power Delivery*, vol. 12, no. 2, pp. 965-970, April 1997.

[8] C. de Toureil et al., "Review of in service diagnostic testing of composite insulators," Tech. Rep.WG 22.03: Insulators.

[9] G. H. Vaillancourt, J. P. Bellerive, M. St-Jean, and C. Jean, "New live line tester for porcelain suspension insulators on high voltage power lines," *IEEE Trans. Power Delivery*, vol. 9, no. 1, pp. 208-219, Jan. 1994.

[10] G. H. Vaillancourt, S. Carignan, and C. Jean, "Experience with the detection of faulty composite insulators on high voltage power lines by the electric field measurement method," *IEEE Trans. Power Delivery*, vol. 13, no. 2, pp. 661-666, Apr. 1998.

[11] "Positron insulator tester," Positron industries Inc., Canada, 2003

[12] G. H. Vaillancourt, M. Hamel and J. Frate, "Experience with two faulty composite insulators detection methods in hydro-Québec," *10th International Symposium on High Voltage Engineering*, Aug.1997

[13] E. Spangenberg, and G. Riquel, "In service diagnostic of composite insulators EDF's test results," *10th International Symposium on High Voltage Engineering*, Aug. 1997.